Measurement of convergence in plane-wave migration

Chad M. Hogan and Gary F. Margrave

ABSTRACT

We have developed a FOCI-driven imaging code that implements a plane-wave migration algorithm. This algorithm produces images that are interpretable with a fraction of the computation time required for a full prestack migration. Additionally, the image may be selectively refined to maximize the benefit of computation time. To guide this refinement, we propose a measure ("residual") of the convergence of the imaging. This method selects a region of the image to monitor. Then within this region, the ℓ^2 norm of the difference between two successive plane-wave stacks normalized by the ℓ^2 norm of the first plane-wave stack is calculated. This residual decreases rapidly while the image is improving and approaches zero as the image approaches its limit.

We have implemented this plane-wave code in order to facilitate highly-efficient prestack wave-equation depth migration. Although plane-wave migration is well-known in the seismic community, we intend to use this code as a starting point for future theoretical developments.

INTRODUCTION

Prestack depth migration is costly for complex regions with strong lateral velocity variations. In these regions, it is desirable to use a wave-equation migration algorithm such as FOCI (Margrave et al., 2006). Plane-wave migration was in part developed to preserve the fidelity benefits of prestack wave equation techniques while adding the benefits of poststack processing economy (see e.g. Rietveld et al., 1992; Whitmore, 1995; Mosher and Foster, 1998; Duquet et al., 2001; Liu et al., 2002, 2006). Physically, the method may be seen as an application of Huygens' principle. A plane wave is synthesized by the superposition of numerous point sources. In terms of seismic imaging, this may be accomplished by stacking common shot gathers that are time-delayed by a linear function of the shot location. This stack is imaged using a similarly constructed plane wave source model. A zero time-delay corresponds to a horizontal plane wave (i.e. with $0°$ orientation). Positive and negative time-delays correspond to plane waves with positive and negative orientation.

In contrast to usual shot-profile migration, plane-wave migration has the benefit that, in many cases, a useful image can be developed from relatively few individual plane waves. In the case of flat homogeneous layers and a seismic survey with numerous shots and receivers, it is conceivable that only the $0°$ plane wave could be required to generate a usable image. This is roughly equivalent in cost to a poststack migration. However, plane-wave migration has the added benefit that more plane waves with varying orientation may be added at any time to selectively improve the image. This allows fine control of the overall cost of imaging, and allows individuals to choose precisely where they would like to spend their time in imaging.

The algorithm we have implemented is an extension of the CREWES FOCI code. It retains all features of FOCI including operator stabilization and spatial resampling, but adds

the ability to stack shot records into plane-wave gathers and use the requisite plane-wave source model.

THEORY

The theory of plane-wave migration is explained by several authors. Here we select several important concepts as described by Liu et al. (2006). A similar treatment may also be found in Romero et al. (2000).

Consider a source wavefield of a shot $S_j(\omega, x, z)$, where ω is temporal frequency, x is the lateral spatial coordinate, z is spatial coordinate below the surface, and index $j = 1, 2, \ldots N$ where N is the total number of shots. A composite wavefield $\bar{S}(\omega, x, z)$ is expressed as

$$\bar{S}(\omega, x, z) = \sum_{j=1}^{N} a_j(\omega) S_j(\omega, x, z) \tag{1}$$

where the $a_j(\omega)$ are N functions that serve to time-delay shots as required via time-delay/phase-shift equivalency. Similarly, we may consider a composite receiver wavefield $\bar{R}(\omega, x, z)$,

$$\bar{R}(\omega, x, z) = \sum_{j=1}^{N} a_j(\omega) R_j(\omega, x, z). \tag{2}$$

$R_j(\omega, x, z)$ is the backward-extrapolated receiver wavefield that corresponds to $S_j(\omega, x, z)$.

Compose a 2D plane-wave section simulating a line-source wavefield with ray parameter p,

$$a_j(\omega) = f(\omega) e^{i\omega p(x_j - x_0)} \tag{3}$$

where $f(\omega)$ is a real function, and x_0 is the plane wave origin at the surface.

For wavefield extrapolation operators, Liu et al. (2006) define $\mathcal{L}$ and its conjugate operator $\mathcal{L}^*$ such that

$$S(\omega, x, z) = \mathcal{L}^*[S(\omega, x, z - \Delta z)] \tag{4}$$
$$R(\omega, x, z) = \mathcal{L}[R(\omega, x, z - \Delta z)] \tag{5}$$

Application of $\mathcal{L}$ to $\bar{S}$ and $\bar{R}$ gives

$$\bar{S}(\omega, x, z) = \mathcal{L}^*[\bar{S}(\omega, x, z - \Delta z)], \tag{6}$$
$$\bar{R}(\omega, x, z) = \mathcal{L}[\bar{R}(\omega, x, z - \Delta z)]. \tag{7}$$

Use of a crosscorrelation imaging condition yields an image $I(x,z)$,

$$I(x,z) = \sum_\omega \bar{S}^*(\omega,x,z)\bar{R}(\omega,x,z) \tag{8}$$

$$= \sum_{j=1}^{N}\sum_\omega |a_j(\omega)|^2 S_j^*(\omega,x,z)R_j(\omega,x,z) \tag{9}$$

$$+ \sum_{j\neq k}^{N}\sum_\omega a_j^*(\omega)a_k(\omega)S_j^*(\omega,x,z)R_k(\omega,x,z)$$

Liu et al. (2006) describe each term in equation 9. The first is the stack of images for each individual shot, which is the expected output from a shot-profile migration. The second term is described as the results of the crosscorrelation of source wavefields with the receiver wavefields from different shots – "cross terms". This results in an imaging artifact which is traditionally addressed with phase encoding techniques (e.g. Romero et al., 2000).

2D source plane-wave migration

If equation 3 is substituted into equation 9, Liu et al. (2006) show that the image generated by a single plane-wave section $I_p(x,z)$ is

$$I_p(x,z) = \sum_\omega f^2(\omega)\sum_{j=1}^{N}\sum_{k=1}^{N} e^{i\omega p(x_j-x_k)}S_k^*(\omega,x,z)R_j(\omega,x,z), \tag{10}$$

that, upon stacking all source plane waves, the final image $I(x,z)$ is

$$I(x,z) = \sum_{p=-N_p}^{N_p} I_p(x,z)$$

$$= \sum_{j=1}^{N}\sum_{k=1}^{N}\sum_\omega f^2(\omega)S_k^*(\omega,x,z)R_j(\omega,x,z)\sum_{l=-N_p}^{N_p} e^{i\omega l\Delta p(x_j-x_k)}, \tag{11}$$

and that the final sum in equation 11 approximates a delta function,

$$\lim_{N_p\to\infty}\sum_{l=-N_p}^{N_p} e^{i\omega l\Delta p(x_j-x_k)} = |\omega|^{-1}\delta(x_j-x_k). \tag{12}$$

This important result demonstrates that, given enough plane waves, the cross terms are suppressed. Also, plane-wave migration is valid even in cases of irregular and sparsely-sampled data sets. Liu et al. (2006) also make the point that the computational savings in plane-wave migration are likely to be found in large data sets. The number of plane waves required to suppress these artifacts is roughly a constant for a given physical volume to image, independent of the actual number of shot records in that volume.

Residuals

The question remains, how many plane waves are enough? We propose a simple measure of convergence. This residual is defined in terms of two successive plane-wave images, $I_N(x, z)$ and $I_{N+1}(x, z)$. N may refer to any ordering of plane-wave images. For example, $I_N(x, z)$ refers to the image generated by the stacking of 11 distinct plane wave images, while $I_{N+1}(x, z)$ refers to the image generated by the stacking of 13 distinct plane wave images.* These two images will be spatially localized by a window $\Omega(x, z)$, with a value of one inside the region of interest, zero when well outside, with a smooth transition between inside and outside. This windowing allows the algorithm to focus on a specific portion of the image, perhaps shallow or deep, perhaps in complex or simple structure.

Specifically, the residual $\mathcal{R}(x, z)$ is calculated as

$$\mathcal{R}(x, z) = \frac{\sqrt{\sum_{x,z} \Omega(x, z)(I_{N+1}(x, z) - I_N(x, z))^2}}{\sqrt{\sum_{x,z} \Omega(x, z)(I_N(x, z))^2}} \tag{13}$$

TESTING

Simple synthetic

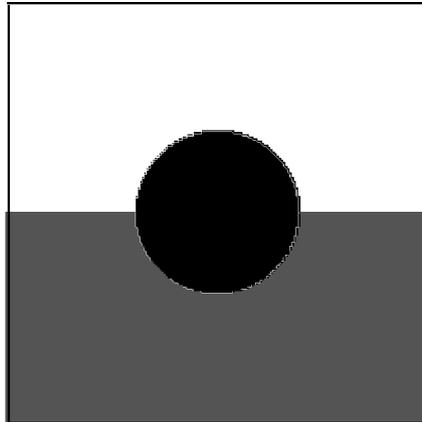We tested the algorithm on the velocity model shown in Figure 1. This model was

FIG. 1. Velocity model. The white region represents a relative velocity of 4, grey represents 6, and black represents 3.

chosen to provide a continuous range of dip in order to highlight the various plane-wave incident angles, and the effectiveness of varying numbers of plane-wave images.

The simulated seismic model data consisted of 51 equally spaced shots spanning the surface of the model recorded into 200 equally spaced receivers which also spanned the

---

*In this implementation for the sequence, plane waves are added symmetrically, two at a time. Therefore, the 13 plane-wave image is the successor to the 11 plane-wave image.

surface. The data was generated with the CREWES `afd_shotrec` finite difference modelling facility.

Figure 2 shows an image of this velocity model calculated with a standard FOCI shot-profile migration. The horizontal contact is easily visible. It appears that dips up to approximately 30° of the circle are visible as well. The shot-profile image here does not show the steep sizes of the circle due to a lack of adequate direct scattering of energy back to the surface.
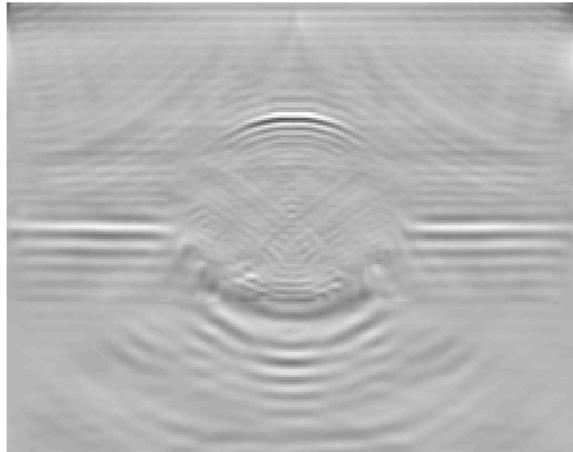

FIG. 2. An image of the velocity model calculated with shot-profile migration.

Figure 3 shows the plane wave image generated using only the horizontal plane wave. This is roughly equivalent in computation time to a poststack migration. A significant
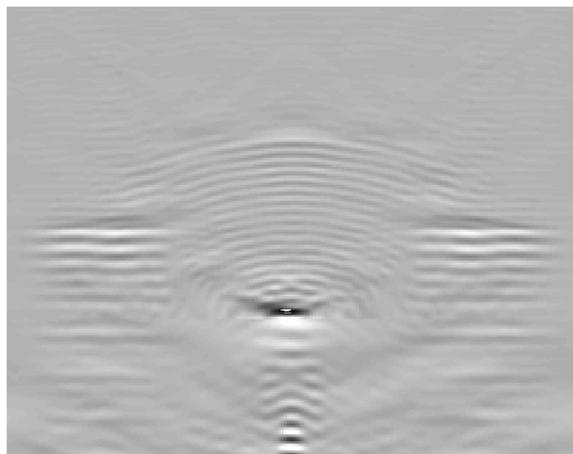

FIG. 3. The horizontal plane wave image.

portion of the image is recognizable, though it is hardly equivalent to the full shot-profile image. Figure 4 shows the addition of plane waves at ±31°. With just three plane waves, we have clearly revealed the gross structure of the model including the same ±30° dip limits on the top of the circle. As seen in Figure 4, the addition of plane waves at ±11° clarifies the image and removes noise, especially for the horizontal contact. With two more plane
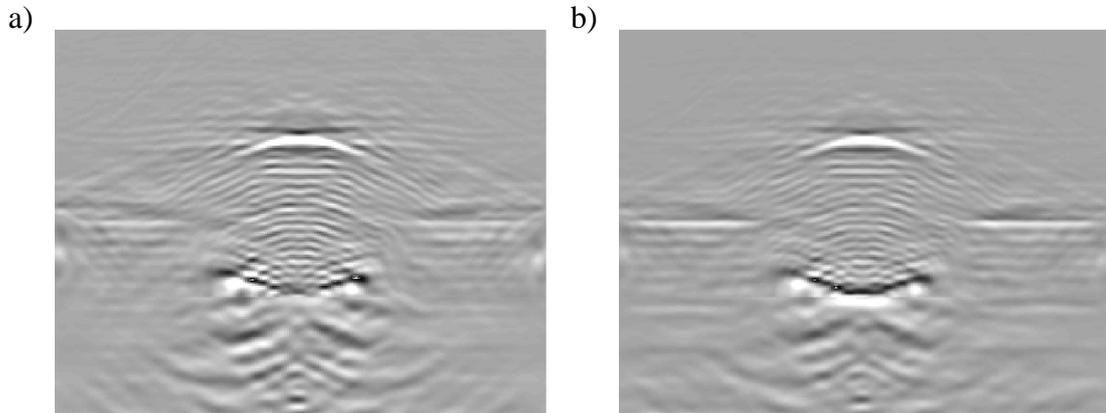
a)   b)

FIG. 4. Plane-wave images generated with a) plane waves at $0°, \pm31°$, b) $0°, \pm11°, \pm31°$.

a)   b)
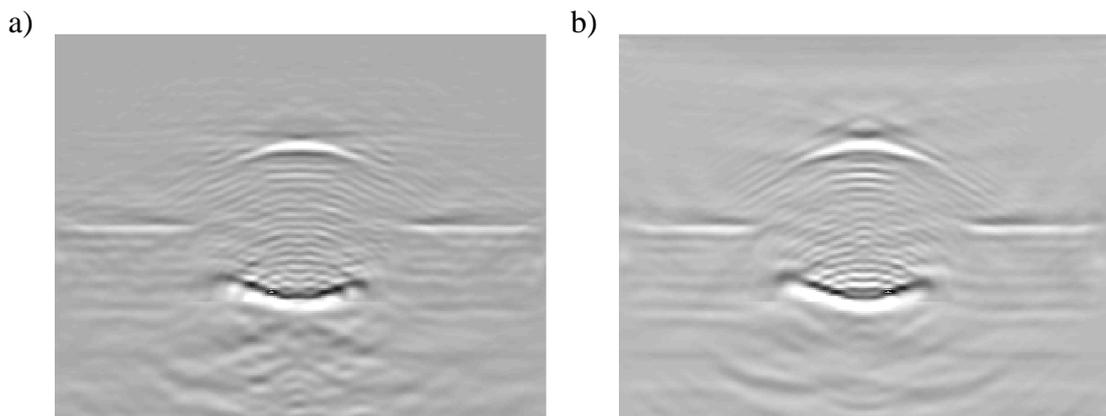

FIG. 5. Plane-wave images generated with a) plane waves at $0°, \pm11°, \pm22°, \pm31°$, b) 51 plane waves between $-31°$ and $+31°$.

waves at $\pm22°$, the image in Figure 5 clarifies even more, though no significant structure is revealed.

Finally, in Figure 5, 51 plane waves ranging between $+31°$ and $-31°$ are used to generate an image of comparable computational cost to the shot-profile migration, which required the migration of 51 shot records.

Marmousi testing

Testing of this method on the Marmousi velocity model (Figure 6) showed an interpretable image that emerged from very few plane waves. Residuals were calculated following equation 13 for the region at approximately $(6500, 2400)$, and are shown in Figure 7. First, we notice that the plane-wave migration seems to converge to its final form much faster than the shot-profile migration. Second, we notice that the plane-wave image stops improving dramatically with the use of 41 plane waves, and essentially stops improving at 81 plane waves. At this point, the plane-wave migration was halted as no improvement was evident. The shot-profile migration continues to benefit from additional shots throughout the entire 240 shots, though the major improvement slows at around 110 shots. Figure 8 shows shot-profile migration with 110 shots compared to its final state at 240 shots. Fig-
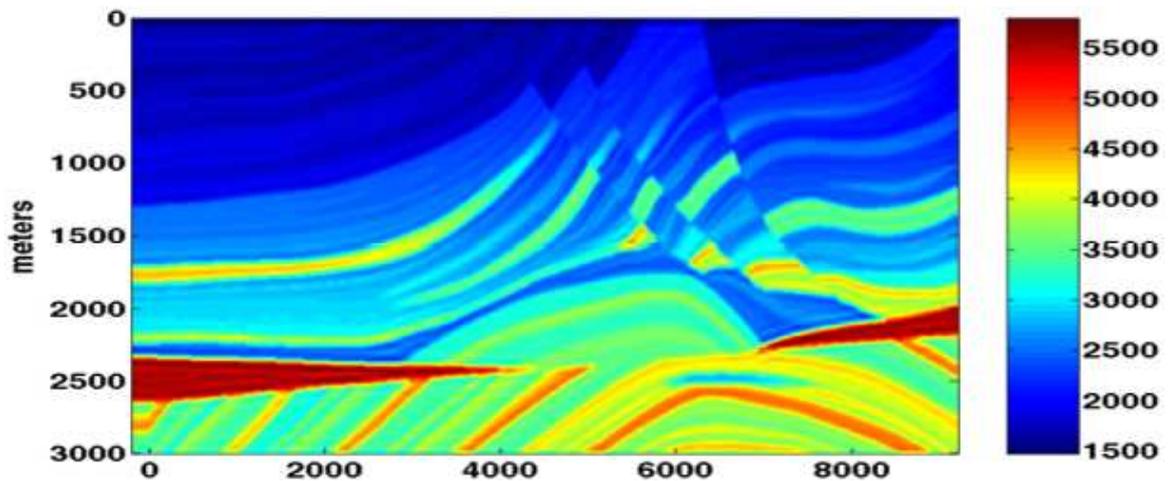
FIG. 6. The Marmousi velocity model. Velocity ranges from 1500 m/s to 6000 m/s.

ure 9 compares the result from 41 plane waves to the result from 41 shots, and Figure 10 compares the result from 81 plane waves to the result from 81 shots.
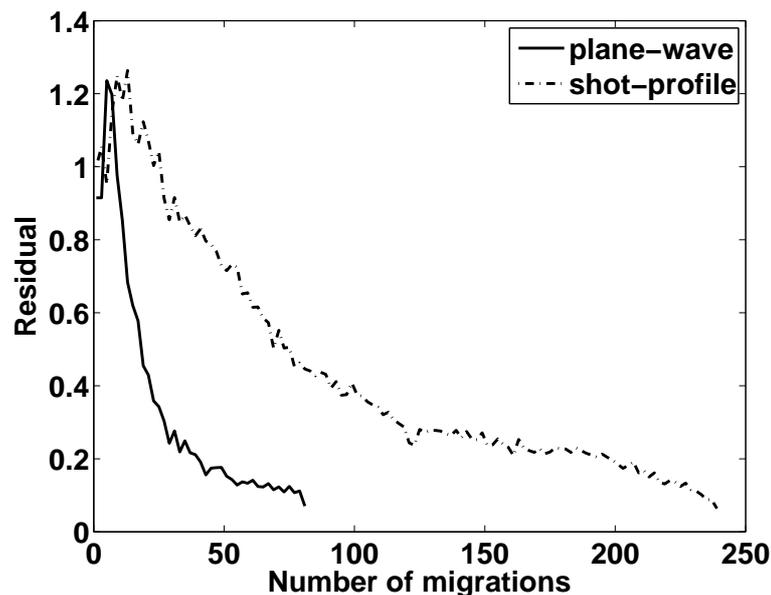

FIG. 7. Residuals for shot-profile and plane-wave migration as a function of number of individual migrations (i.e. number of plane waves or number of shot records migrated). The plane-wave residuals show dramatically faster reduction in residual, compared to the slower decline in shot-profile migration.

However, the plane-wave migration images seem to suffer from a lack of high-frequency resolution in the fine details of the images, and very little improvement in the image quality is observed with more than 81 plane waves.

Converging, but to what?

Figure 7 clearly shows the plane-wave imaging converging to its final result faster than shot-profile migration. The obvious question is then, is plane-wave migration converging to
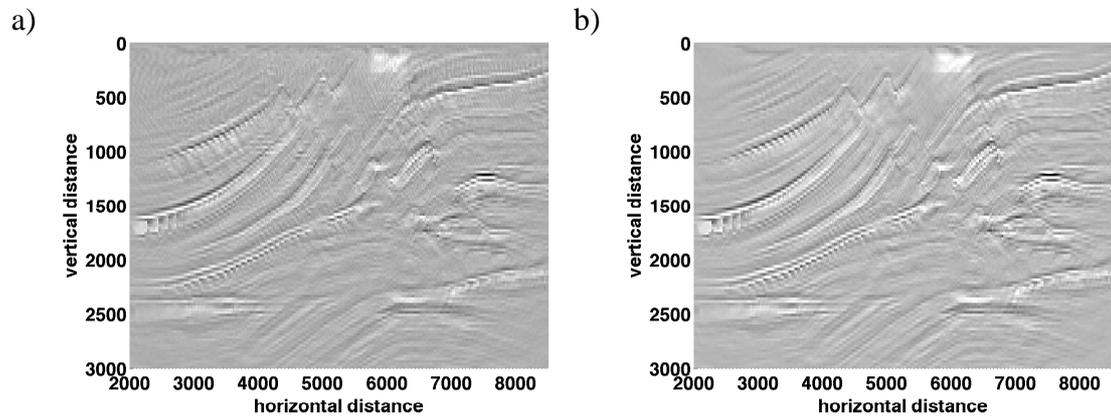
a)   b)

FIG. 8. Marmousi shot-profile migration with a) 110 shot records and b) 240 shot records.
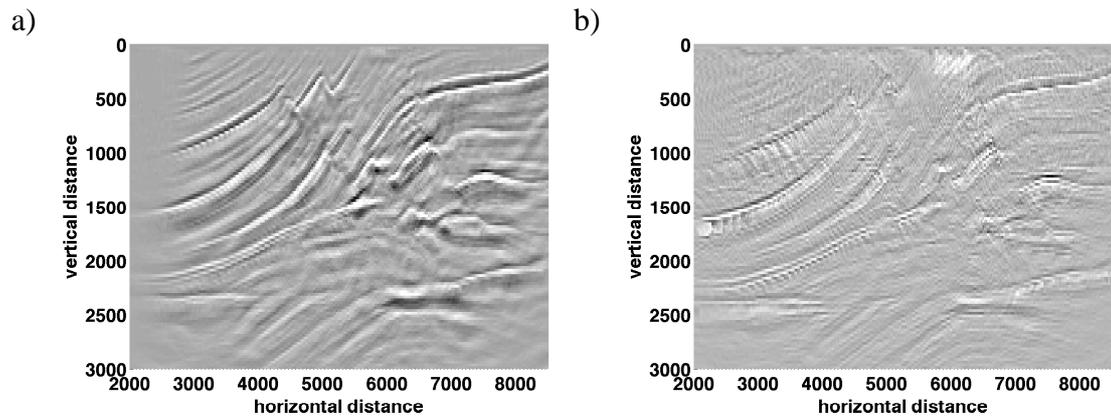
a)   b)

FIG. 9. Marmousi migration with a) 41 plane waves and b) 41 shot records.
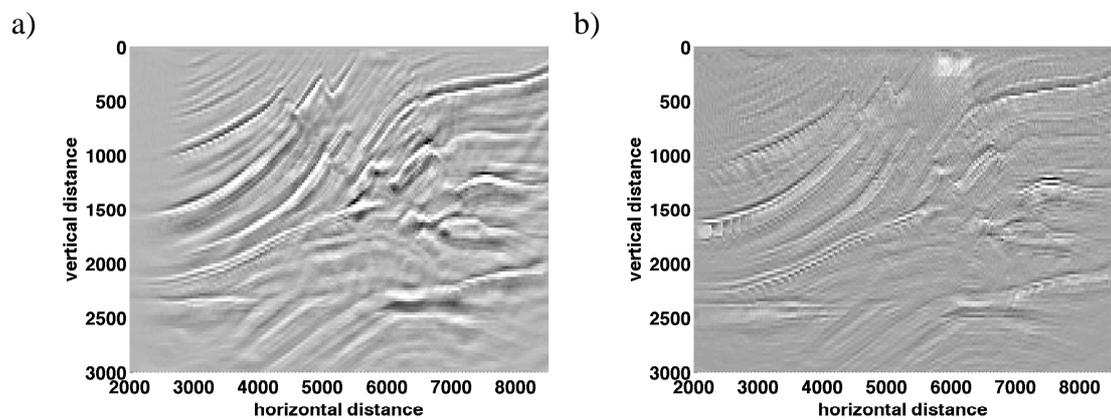
a)   b)

FIG. 10. Marmousi migration with a) 81 plane waves and b) 81 shot records.

the "correct" final image? To test this, we first accept that the shot-profile migration calculated with 240 shots (Figure 8) is clearly superior to the final plane-wave image calculated with 81 plane waves (Figure 10). We then calculate the residual between an intermediate calculation and this 240-shot image. These residuals are shown in Figure 11. Although the final plane-wave image does not have the fine detail of the final shot-profile image, it is clear that the plane-wave image approaches the final shot-profile image much faster than the shot-profile image itself converges. That is, the 81 plane-wave image has a significantly lower residual than the 81 shot image. In fact, the full numerical results reveal that the shot-profile image requires 175 shots to reach the same level of residual as the 81 plane-wave image.
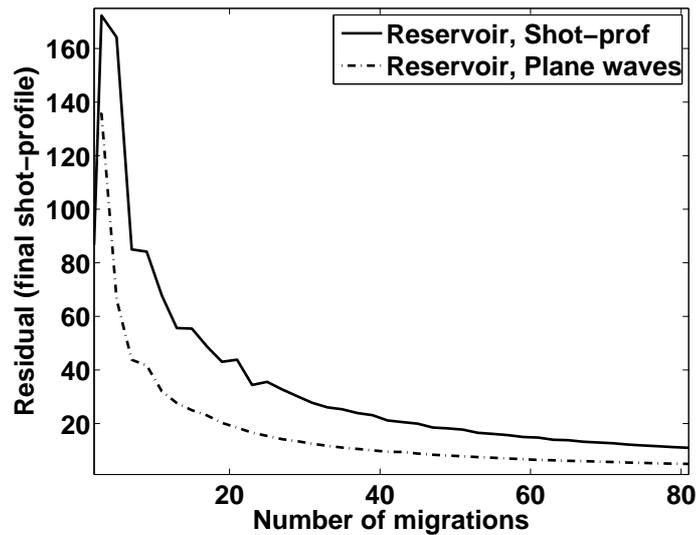

FIG. 11. Residual calculated between an intermediate image and the final "best" image calculated with 240 shots.

DISCUSSION

The plane-wave migration resolves the image efficiently, requiring only a few plane waves to adequately resolve the structure. The single horizontal plane-wave image suggested the placement of the horizontal contact, and hinted at the location of the top of the circle feature. With the addition of two plane waves at approximately $+30°$ and $-30°$, however, the horizontal contact and a great deal of the shape of the circle were clearly revealed. Optimal results appear to manifest at 7 plane waves. The qualitative difference between using 7 plane waves and 51 plane waves is small, so with plane-wave migration a comparable image can be calculated in this case in something like 15% of the original shot-profile migration calculation time.

The final process using 51 plane waves did not result in an image of the same quality as the shot-profile migration. This suggests that the algorithm as implemented is somehow suboptimal. One possible shortcoming is the method for choice of plane waves to use in migration. This issue was explored for real data by Stork and Kapoor (2004), who specifically wondered about how many plane waves may be required for reliable imaging. In this experiment, plane waves were chosen in an ad hoc fashion, simply based on a

constant increment of the time-delays used to create the effective plane waves. Perhaps a more careful algorithm for the selection of plane wave distribution could be developed in order to optimize the imaging.

The Marmousi migration yielded similar results. The plane-wave image very quickly converged to a final image that was not as clear as the final shot-profile migration. However, the plane-wave method revealed a useful image with significantly fewer migrations than the shot-profile image. It is expected that the quality of the final plane-wave image is strongly dependent on the number of shot and receiver locations. It is in situations of very fine spacing that plane-wave migration is expected to yield its best value in the sense that the number of plane-waves required to produce an image stays nearly constant, but the quality improves with finer sampling. This contrasts with shot-profile migration, in which many more shots would directly require a similar increase in the number of migrations.

CONCLUSIONS AND FUTURE WORK

Plane-wave migration is useful for efficient prestack depth wave-equation migration. By generating effective plane waves and using a plane wave source model, a standard wave-equation algorithm can be easily adapted to plane-wave migration. Though it is relatively straight-forward to implement such an algorithm, other details, such as the number of plane waves to use and specific orientation of these plane waves, remain unsolved problems in many cases.

The residual measure introduced here may be useful in many situations. In addition to giving a numerical measure of when performing more calculation (in the form of adding more plane waves to the image) leads to diminishing returns, there are other possible uses. This residual may be used to guide the selection of the actual plane waves used in migration. In the case of asymmetric geology, for example, it may be desirable to use an angular range of, say, $-30°$ to $+5°$. The residual may also be used to guide focused illumination of a particular geologic feature. For example, the residual may be used to determine which plane waves enhance the imaging of salt flanks, subsalt features, or other poorly-illuminated regions.

REFERENCES

Duquet, B., Laily, P., and Ehinger, A., 2001, 3D plane wave migration of streamer data: 71st Annual International Meeting: SEG, Expanded Abstracts.

Liu, F., Hanson, D., Whitmore, N., Day, R., and Stolt, R., 2006, Toward a unified analysis for source plane-wave migration: Geophysics, **71**, No. 4, S129–S139.

Liu, F., Stolt, R., H.W.Hanson, D., and Day, R., 2002, Plane wave source composition: an accurate phase encoding scheme for prestack migration: 72nd Annual International Meeting: SEG, Expanded Abstracts.

Margrave, G. F., Geiger, H. D., Al-Saleh, S. M., and Lamoureux, M. P., 2006, Improving explicit depth migration with a stabilizing Wiener filter and spatial resampling: Geophysics, **71**, S111–S120.

Mosher, C., and Foster, D., 1998, Offset plane wave propagation in laterally varying media, *in* Mathematical Methods in Geophysical Imaging V: Proceedings of SPIE 3453, 36–46.

Rietveld, W., Berkhout, A., and Wapenaar, C., 1992, Optimum seismic illumination of hydrocarbon reservoirs: Geophysics, **57**, 1334–1345.

Romero, L., Ghiglia, D., Ober, C., and Morton, S., 2000, Phase encoding of shot records in prestack migration: Geophysics, **65**, 426–436.

Stork, C., and Kapoor, J., 2004, How many P values do you want to migrate for delayed-shot wave equation migration?: 74th Annual International Meeting: SEG, Expanded Abstracts.

Whitmore, N., 1995, An imaging hierarchy for common angle plane wave seismograms: Ph.D. thesis, University of Tulsa.